M A T H E M A T I C S D E P A R T M E N T

Application of the Taylor-Galerkin Method to Transport Problems in Subsurface Hydrology

K.J. Neylon

Numerical Analysis Report 5/93

U N I V E R S I T Y O F R E A D I N G

Application of the Taylor-Galerkin Method to Transport Problems in Subsurface Hydrology

K.J. Neylon

Numerical Analysis Report 5/93

Department of Mathematics
P.O. Box 220
University of Reading
Whiteknights
Reading
RG6 2AX
United Kingdom

Abstract

A model for saline intrusion - an example of non-passive, non-reactive, single-species contaminant transport in a porous medium - is presented. A computational algorithm for approximating the solution of this contaminant transport model is given.

An implicit Taylor-Galerkin method is used to discretise the contaminant continuity equation (which takes the form of an advection-diffusion equation). This discretisation method gives a non-symmetric matrix system (due to the fully implicit treatment of the advection term) which is solved by the Bi-CGSTAB non-symmetric iterative method. The performance of the Bi-CGSTAB solver is not considered in this work.

This algorithm is tested on two test cases from the literature; the first involves the 1-D transport of a tracer in a vertical column (for which an analytic solution is available) and the second, which is more specific to the problem of saline intrusion, is the Henry problem. The method is shown to give transient results which agree well with both analytic solutions and those from the literature.

Contents

1 Introduction

This report is concerned with the numerical modelling of non-passive, non-reactive, single-species contaminant transport in saturated porous media. In this type of flow, a contaminant is carried through a porous medium by a fluid; the contaminant does not undergo any chemical or biological reactions but its presence does affect the physical properties of the fluid, e.g. density, viscosity.

A common example of this type of flow is saline intrusion - saltwater moving inland and mixing with less dense freshwater. In regions where coastal aquifers are utilised for water supply, saline intrusion leads to a degradation of groundwater quality. To control this, an accurate and reliable model for the shape and position of the saltwater front is required to predict the response to changes in usage patterns. A solution of this type of problem is the object of this work.

There is a transition zone between the freshwater and the saltwater caused by hydrodynamic dispersion. In some circumstances, the width of this zone is small relative to the thickness of the aquifer so that it may be approximated as a sharp interface [1]. This report is concerned with flows in which the sharp interface approximation is not valid and a full variable density model must be used.

Variable density transport models are well documented in the literature. They consist of three main components : a fluid continuity equation which models the fluid flow, a contaminant continuity equation which models the contaminant behaviour, and a constitutive equation which relates the contaminant concentration to the fluid density. In general, it is not possible to solve these governing equations analytically so numerical methods are necessary to approximate the solution.

Most of the current approaches use the finite element method to discretise the problem spatially, since this allows good representation of geometrically complex physical features in the domain. The finite element method is used to perform the spatial discretisation in this work.

One of the main differences between the numerical schemes in the literature is the approach used to treat the contaminant transport part of the model. A standard Galerkin finite element spatial approximation with fully implicit time-stepping leads to a discretised system which is non-symmetric due to the implicit treatment of the advection term [9, 15, 17]. These non-symmetric matrix systems tend to be more computationally expensive to solve than symmetric ones.

Symmetry can be achieved by the use of fully explicit methods, but these lead

to restrictions on the size of the discrete time step to ensure stability - making these methods unfeasible for long term transient calculations. Symmetry is also possible by the use of operator splitting which allows the advection component of the equation to be treated explicitly while the other terms are treated implicitly (e.g. [3, 10]) or by the use of Lagrangian methods which effectively follow particles along characteristics to solve the advection component (e.g. [7]).

However, due to recent developments in non-symmetric matrix solvers (e.g. GMRES [14], Bi-CGSTAB [16]), the solution of non-symmetric matrix systems is not as computationally expensive as was once the case. In this report, an implicit Taylor-Galerkin method [5] is used to discretise the contaminant continuity equation, the non-symmetric system which results is solved using Bi-CGSTAB. The performance (i.e. convergence, stability, computational efficiency, etc.) of the Bi-CGSTAB method will be investigated in a future report and so is not considered here.

In the following section, a mathematical model for non-passive, non-reactive, single-species contaminant transport in saturated porous media is described. In Section 3 an implicit Taylor-Galerkin method for advection-diffusion equations is introduced. It is shown that this scheme is equivalent to the well-known Crank-Nicolson finite element method. A full description of the numerical scheme for solving the equations which comprise the mathematical model is given in Section 4 and the performance for two test problems is presented in Section 5.

2 Governing Equations

In non-passive contaminant transport, the presence of the contaminant affects the properties of the fluid; it is assumed that only the density of the fluid is affected in this work. The contaminants considered are non-reactive so there are no chemical effects to consider. A mathematical model which governs flows of this type in porous media can be formulated in terms of

1. a continuity equation for the fluid,
2. a continuity equation for the contaminant, and
3. a constitutive equation,

with the relevant initial and boundary conditions.

2.1 Fluid Continuity Equation

It is convenient to write the fluid continuity equation in terms of either the pressure, p, or the piezometric head, h, defined as

$$h = \frac{p}{\rho g} + z,$$

where $\rho = \rho(c)$ is fluid density (ML^{-3})
c is the (dimensionless) contaminant concentration
g is acceleration due to gravity (MLT^{-2})
z is the elevation above a datum (positive upwards) (L) ,

since these variables are continuous across the contaminated/contaminant-free interface and so apply as single state variables over the whole domain.

If it is assumed that the porous medium is non-deformable and the Reynolds number of the flow is not so large as to invalidate Darcy's law, then the fluid flux equation is given by a generalised form of Darcy's equation [1],

$$\mathbf{q} = -\underline{\underline{\mathbf{k}}} \left(\nabla p + \rho g \nabla z \right) / \mu,$$

where $\mathbf{q}$ is the Darcy velocity vector (LT^{-1})
$\underline{\underline{\mathbf{k}}}$ is the permeability tensor (L^2)
μ is the dynamic viscosity of the fluid ($\mathrm{ML}^{-1}\mathrm{T}^{-1}$) .

In this work, it is assumed that μ is constant and equal to the viscosity of the non-contaminated fluid, μ_0. Hence the fluid flux equation can be written in terms of the piezometric head as

$$\mathbf{q} = -\underline{\underline{\mathbf{K}}} \left\{ \nabla h + (h - z) \frac{\nabla \rho}{\rho} \right\}, \tag{1}$$

where $\underline{\underline{\mathbf{K}}} = \frac{\underline{\underline{\mathbf{k}}} \rho g}{\mu_0}$ is the hydraulic conductivity tensor (LT^{-1}). From [1], in the absence of source terms the fluid mass balance equation for saturated flow (i.e. flow in which the moisture content is equal to the porosity and hence independent of time) is

$$\phi \frac{\partial \rho}{\partial t} + \nabla . (\rho \mathbf{q}) = 0, \tag{2}$$

where ϕ is the porosity of the porous medium. Substitution of $\mathbf{q}$ from (1) into (2) constitutes the fluid continuity equation.

2.2 Contaminant Continuity Equation

From [1], in the absence of source terms the contaminant mass balance equation for saturated flow is

$$\phi \frac{\partial (\rho c)}{\partial t} + \nabla . \left\{ \rho c \mathbf{q} - \phi \underline{\underline{\mathbf{D}}} \nabla (\rho c) \right\} = 0, \tag{3}$$

where $\underline{\underline{\mathbf{D}}} = \underline{\underline{\mathbf{D}}}(\mathbf{q})$ is the dispersion tensor ($\mathrm{L}^2\mathrm{T}^{-1}$). The (i, j) entry in the dispersion tensor is related to the i and j components of the fluid velocity vector, $\mathbf{v}$ $(= \mathbf{q}/\phi)$, by

$$D_{ij} = (\alpha_T |\mathbf{v}| + D_m)\, \delta_{ij} + (\alpha_L - \alpha_T) \frac{v_i v_j}{|\mathbf{v}|},$$

where α_T is the transverse dispersivity (L)

α_L is the longitudinal dispersivity (L)

D_m is the coefficient of molecular diffusion ($\mathrm{L}^2\mathrm{T}^{-1}$)

$\delta_{ij} = 1$ for $i = j$, zero otherwise.

Substitution of $\mathbf{q}$ from (1) into (3) constitutes the contaminant continuity equation.

2.3 Constitutive Equation

The constitutive equation relates the fluid density to the contaminant concentration. In this work the density is assumed to be a linear function of the concentration, i.e.

$$\rho = \rho_0 + \frac{\partial \rho}{\partial c} c, \tag{4}$$

where ρ_0 is the density of the non-contaminated fluid (ML^{-3})

$\frac{\partial \rho}{\partial c}$ is treated as a constant (ML^{-3}) .

2.4 Initial and Boundary Conditions

For the fluid continuity equation, the initial condition is

$$h = h_0 \qquad \text{on } \Omega,$$

where Ω is the spatial domain and the boundary conditions are

$$\begin{aligned} h &= \tilde{h} \quad \text{on} \quad \Gamma_1 \quad \text{(prescribed head)} \\ -\mathbf{q}.\mathbf{n} &= q_n^h \quad \text{on} \quad \Gamma_2 \quad \text{(prescribed fluid flux),} \end{aligned}$$

where $\mathbf{n}$ is the unit outward normal vector and Γ is the boundary of Ω (and $\Gamma_1 + \Gamma_2 = \Gamma$). For the contaminant continuity equation, the initial condition is

$$c = c_0 \qquad \text{on } \Omega,$$

and the boundary conditions are

$$\begin{aligned} c &= \tilde{c} \quad \text{on} \quad \Gamma_1' \quad \text{(prescribed concentration)} \\ -\phi \underline{\underline{\mathbf{D}}} \nabla(\rho c).\mathbf{n} &= q_n^c \quad \text{on} \quad \Gamma_2' \quad \text{(prescribed dispersive solute mass flux)} \end{aligned}$$

(where $\Gamma_1' + \Gamma_2' = \Gamma$).

The convention used for the sign of both the prescribed fluid flux and the prescribed dispersive solute mass flux is that they are positive if the flow is directed into the region.

3 The Taylor-Galerkin Method

The contaminant mass balance equation (3) is an advection-diffusion equation. In this report, the advection-diffusion equation is discretised by the Taylor-Galerkin method [5, 6]. This method for generating a fully discretised equation consists of three stages. In the first stage, the first order temporal derivative is approximated using a Taylor series expansion of the solution variable in time (including higher order temporal derivatives). In the second stage, as many of the temporal derivatives as possible are replaced by spatial derivatives using the advection-diffusion equation itself, the remaining temporal derivatives being neglected. This leads to a temporally discretised equation. In the final stage, the spatial derivatives are discretised by the standard Galerkin finite element method.

In the literature the Taylor-Galerkin method has already been applied to environmental modelling problems with some degree of success, e.g. the shallow water equations [13]. Essentially, it is the finite element version of the well-known Lax-Wendroff scheme; hence it is also susceptible to oscillations near discontinuities. These situations are not expected in the flows considered in this work so this is not a serious problem.

In this section, the Taylor-Galerkin method is introduced for the scalar wave equation and applied to the scalar advection-diffusion equation, results being given on the accuracy and stability of the method.

3.1 Pure Advection Equation

As the Taylor-Galerkin method was originally introduced for the pure advection problem [5], it is most natural to introduce the method in this framework. Consider the one-dimensional scalar wave equation,

$$\frac{\partial u}{\partial t} + a\frac{\partial u}{\partial x} = 0 \qquad \text{on } x \in \Omega, \tag{5}$$

where a is a constant and $u = u(x,t)$. The Taylor series expansion of $u(x, t+\Delta t)$ about t is

$$u(x,t+\Delta t) = u(x,t) + \Delta t\frac{\partial u}{\partial t}(x,t) + \frac{(\Delta t)^2}{2!}\frac{\partial^2 u}{\partial t^2}(x,t) + \mathrm{O}(\Delta t)^3.$$

Using (5) to replace the temporal derivatives by spatial ones gives (to $O(\Delta t)^2$)

$$\frac{u(x,t+\Delta t)-u(x,t)}{\Delta t} = -a\frac{\partial u}{\partial x}(x,t) + a^2\frac{\Delta t}{2}\frac{\partial^2 u}{\partial x^2}(x,t). \qquad (6)$$

This is an explicit temporally discretised form of (5). Any spatial discretisation can be chosen at this stage; centred finite differences lead to the Lax-Wendroff scheme. For the Taylor-Galerkin method, the spatial discretisation is by the standard Galerkin finite element method, i.e. take the weak form of (6) (obtained by multiplying it by a test function, N_i, and integrating over the spatial domain, Ω) and approximate $u(x,t)$ by the finite dimensional expansion

$$u(x,t) \approx \sum_j^{nodes} N_j(x)U_j(t),$$

where N_j are finite element basis functions (which are the same as the test functions) and U_j are nodal approximations to the variable u. This leads to the fully discretised equation

$$\begin{aligned}\frac{1}{\Delta t}\sum_j^{nodes}\{U_j(t+\Delta t)-U_j(t)\}\int_\Omega N_iN_j d\Omega \quad &= \\ -a\sum_j^{nodes} U_j(t)\int_\Omega N_i\frac{\partial N_j}{\partial x}d\Omega \quad &+ \quad a^2\frac{\Delta t}{2}\sum_j^{nodes} U_j(t)\int_\Omega N_i\frac{\partial^2 N_j}{\partial x^2}d\Omega, \quad \forall i.\end{aligned}$$

The term which contains the second order spatial derivative can be integrated by parts to yield a new term which only contains first order spatial derivatives (and a boundary term).

If piecewise linear basis functions are used on a regular mesh and boundary effects are ignored, a Taylor series expansion shows that this scheme is third order accurate in space and second order accurate in time and a Fourier stability analysis shows that the restriction on the Courant number, ν $(= a\frac{\Delta t}{\Delta x})$, to ensure that the numerical solution is always bounded is

$$\nu^2 \leq \frac{1}{3}.$$

3.2 Advection-Diffusion Equation

A Taylor-Galerkin method for the advection-diffusion equation was given in Donea *et al* [6] and proceeds in the same way as the method for the pure advection equation. The example for the pure advection case given in the previous section used a Taylor series expansion of $u(x, t+\Delta t)$ about t and this led to an explicit scheme. In this section, a Taylor series expansion of $u(x,t)$ about $(t+\Delta t)$ (which leads to an implicit scheme) is used.

Consider the one dimensional constant-coefficient advection-diffusion equation,

$$\frac{\partial u}{\partial t} + a\frac{\partial u}{\partial x} - b\frac{\partial^2 u}{\partial x^2} = 0 \qquad \text{on } x \in \Omega, \tag{7}$$

where a and b (> 0) are constants and $u = u(x,t)$. The Taylor series expansion of $u(x,t)$ about $(t+\Delta t)$ is

$$u(x,t) = u(x,t+\Delta t) - \Delta t\frac{\partial u}{\partial t}(x,t+\Delta t) + \frac{(\Delta t)^2}{2!}\frac{\partial^2 u}{\partial t^2}(x,t+\Delta t) - \mathrm{O}(\Delta t)^3$$

From (7), the first partial derivative with respect to time is known, and the second temporal derivative with respect to time is given by

$$\begin{aligned}
\frac{\partial^2 u}{\partial t^2} &= \frac{\partial}{\partial t}\left(\frac{\partial u}{\partial t}\right) \\
&= \left(-a\frac{\partial}{\partial x} + b\frac{\partial^2}{\partial x^2}\right)\left(-a\frac{\partial u}{\partial x} + b\frac{\partial^2 u}{\partial x^2}\right) \\
&= a^2\frac{\partial^2 u}{\partial x^2} - 2ab\frac{\partial^3 u}{\partial x^3} + b^2\frac{\partial^4 u}{\partial x^4}.
\end{aligned}$$

Replacing these temporal derivatives in the Taylor series leads to an implicit, temporally discretised equation, but this contains third- and fourth-order spatial derivatives. The existence of these higher order derivatives prevents the use of linear basis functions. To avoid this problem, the second temporal derivative is replaced by the $\mathrm{O}(\Delta t)$ approximation

$$\frac{\partial^2 u}{\partial t^2}(x,t+\Delta t) \approx \frac{1}{\Delta t}\left\{\frac{\partial u}{\partial t}(x,t+\Delta t) - \frac{\partial u}{\partial t}(x,t)\right\},$$

so that the Taylor series becomes

$$u(x,t) = u(x,t+\Delta t) - \frac{\Delta t}{2}\left\{\frac{\partial u}{\partial t}(x,t+\Delta t) + \frac{\partial u}{\partial t}(x,t)\right\} + \mathrm{O}(\Delta t)^3. \qquad (8)$$

It is interesting to note that the Taylor-Galerkin formulation used here for the advection-diffusion equation leads to a standard Crank-Nicolson temporal discretisation. Using (7) to replace the temporal derivatives by spatial ones gives (to $\mathrm{O}(\Delta t)^2$) the temporally discretised equation

$$\begin{aligned}\frac{u(x,t+\Delta t) - u(x,t)}{\Delta t} &= -\frac{a}{2}\left\{\frac{\partial u}{\partial x}(x,t+\Delta t) + \frac{\partial u}{\partial x}(x,t)\right\} \\ &\quad + \frac{b}{2}\left\{\frac{\partial^2 u}{\partial x^2}(x,t+\Delta t) + \frac{\partial^2 u}{\partial x^2}(x,t)\right\}.\end{aligned}$$

Applying a Galerkin finite element spatial discretisation gives the fully discretised equation

$$\begin{aligned}&\sum_j^{nodes} \frac{1}{\Delta t}\{U_j(t+\Delta t) - U_j(t)\}\int_\Omega N_i N_j d\Omega \\ &= \sum_j^{nodes}\{U_j(t+\Delta t) + U_j(t)\}\left(-\frac{a}{2}\int_\Omega N_i \frac{\partial N_j}{\partial x}d\Omega + \frac{b}{2}\int_\Omega N_i \frac{\partial^2 N_j}{\partial x^2}d\Omega\right), \quad \forall i \qquad (9)\end{aligned}$$

For linear basis functions on a regular mesh, Fourier stability analysis shows that the scheme is unconditionally stable (as expected for an implicit method), and a standard Taylor series expansion shows that the scheme is second order accurate in both space and time, the truncation error, τ, having the form,

$$\tau = \frac{b}{12}(\Delta x)^2\frac{\partial^4 u}{\partial x^4} - \frac{1}{12}(\Delta t)^2\frac{\partial^3 u}{\partial t^3} + (\textit{higher order terms}).$$

An implicit Taylor-Galerkin method is also used in Brusa *et al* [3], but this is an operator splitting implementation in which the advective part is treated explicitly.

Although this leads to a symmetric system, it has the stability restriction of the explicit Taylor-Galerkin method.

In the remainder of this report, the un-split implicit Taylor-Galerkin method for the advection-diffusion equation given by (9) is used in the solution of problems involving transport of non-reactive, single-species contaminants in saturated porous media.

4 Numerical Solution of the Governing Equations

In this section, the methods used to discretise and solve the governing equations from Section 2 are described.

4.1 Partial Coupling

Owing to the dependency of the fluid density, ρ, on the contaminant concentration, c, in the constitutive equation (4), the fluid mass and contaminant mass balance equations are coupled (and the contaminant mass balance equation is non-linear).

In order to solve such a problem, the mass balance equations must either be solved simultaneously with a non-linear iteration (which doubles the order of the problem) or an iteration must be performed between them at each time step, with a non-linear iteration performed on the contaminant mass balance equation during each coupling iteration.

However, in the types of problems considered in this report, the coupling is of a relatively weak nature (i.e. $\frac{\partial \rho}{\partial c}$ is small). Hence, for transient computations, a "partially coupled" approach is adopted in which the term that causes the coupling (the density) is treated explicitly. This linearises the contaminant mass balance equation and also allows the two mass balance equations to be solved separately during each time step [7], dramatically decreasing the complexity and computational cost.

With this partially coupled approach, the structure of each time step is

1. The fluid density at this time step is approximated explicitly by linear extrapolation of the densities from the two previous time steps, i.e.

$$\rho^{n+1} \approx \rho^n + \frac{(\Delta t)^{n+1}}{(\Delta t)^n}(\rho^n - \rho^{n-1}).$$

2. The fluid continuity equation ((1) & (2)) is solved for the piezometric head.

3. The Darcy velocity field is calculated using the fluid flux equation (1).

4. The contaminant mass balance equation (3) is solved for the contaminant concentration.

5. The fluid density is re-calculated from the contaminant concentration using the constitutive equation (4).

The remainder of this section is devoted to the description of steps 2,3 and 4 (steps 1 and 5 being trivial calculations).

4.2 Fluid Continuity Equation

The fluid mass balance equation is spatially discretised using the standard Galerkin finite element method. The weak form of (2) is obtained by multiplying by a test function, ω, and integrating over the whole spatial domain, Ω, i.e.

$$\int_\Omega \left\{ \phi \frac{\partial \rho}{\partial t} + \nabla.(\rho \mathbf{q}) \right\} \omega d\Omega = 0.$$

Applying Green's first identity to the advective term and substituting for $\mathbf{q}$ from (1) gives the weak form of the fluid continuity equation,

$$\int_\Omega \left\{ \omega \phi \frac{\partial \rho}{\partial t} + \nabla \omega.\{ \underline{\underline{\mathbf{K}}} \rho \nabla h + \underline{\underline{\mathbf{K}}} (h - z) \nabla \rho \} \right\} d\Omega = \int_\Gamma \omega \rho q_n^h d\Gamma,$$

where h is the required solution variable and Γ is the boundary of the region Ω. Due to the presence of the $h\nabla\omega$ term, a standard Galerkin finite element spatial discretisation of this equation results in a non-symmetric matrix system. However, following Brusa *et al* [3], this is avoided by making the change of variable

$$\Phi = \rho(h - z),$$

so that the weak form becomes

$$\int_\Omega \left\{ \omega \phi \frac{\partial \rho}{\partial t} + \nabla \omega.\underline{\underline{\mathbf{K}}} (\nabla \Phi + \rho \nabla z) \right\} d\Omega = \int_\Gamma \omega \rho q_n^h d\Gamma.$$

This weak form is temporally discretised by a fully implicit finite difference

method to give

$$\int_\Omega \nabla\omega.\underline{\underline{\mathbf{K}}}^{n+1}(\nabla\Phi^{n+1}+\rho^{n+1}\nabla z)d\Omega+\int_\Omega\frac{\omega\phi}{\Delta t}(\rho^{n+1}-\rho^n)d\Omega=\int_\Gamma\omega\rho^{n+1}q_n^{h,n+1}d\Gamma,$$

where the superscripts denote the discrete time level. This weak form is then spatially discretised by the standard Galerkin finite element method, i.e.

$$\omega = N_I \qquad I=1,\ldots,nodes,$$

and Φ is replaced by the finite dimensional expansion

$$\Phi \approx \sum_{J=1}^{nodes}\Phi_J N_J$$

where *nodes* is the number of nodes in the finite element mesh

Φ_J are the nodal approximations to Φ

N_J are the basis functions .

Approximating the material and fluid properties by their average values on elements (or element faces depending on the region of integration) denoted by $\langle\cdot\rangle$ gives the fully discretised equation

$$A\mathbf{\Phi}^{n+1}=\mathbf{F}-\frac{1}{\Delta t}(\mathbf{G}^{n+1}-\mathbf{G}^n),$$

where

$$A=\{A_{IJ}\}_{I,J=1,\ldots,nodes} \qquad \mathbf{F}=\{F_I\}_{I=1,\ldots,nodes}$$
$$\mathbf{\Phi}^{n+1}=\{\Phi_J^{n+1}\}_{J=1,\ldots,nodes} \qquad \mathbf{G}^i=\{G_I^i\}_{I=1,\ldots,nodes},$$

and

$$A_{IJ} = \sum_e A_{IJ}^e=\sum_e\int_{\Omega^e}\nabla N_I.\langle\underline{\underline{\mathbf{K}}}\rangle^{n+1}\nabla N_J d\Omega^e$$

$$F_I = \sum_e F_I^e=\sum_e\left\{\langle\rho\rangle^{n+1}\langle q_n^h\rangle^{n+1}\int_{\Gamma^e}N_I d\Gamma^e-\langle\rho\rangle^{n+1}\int_{\Omega^e}\nabla N_I.\langle\underline{\underline{\mathbf{K}}}\rangle^{n+1}\nabla z d\Omega^e\right\}$$

$$G_I^i = \sum_e G_I^{e,i}=\sum_e\langle\rho\rangle^i\langle\phi\rangle\int_{\Omega^e}N_I d\Omega^e.$$

After the Dirichlet boundary conditions are applied, the matrix in this system

is symmetic and positive definite if the tensor $\langle \underline{\underline{\mathbf{K}}} \rangle^{n+1}$ is symmetric and positive definite ([4], p212). For a reasonably fine spatial discretisation, the system is also large and sparse so an iterative solution method is preferable. A suitable solution technique is the incomplete Cholesky preconditioned conjugate gradient method (ICCG) [11] which is used in this work.

4.3 Darcy Velocity Calculation

An average value of the Darcy velocity of the fluid on each element, which is needed in the contaminant mass balance part of the model, is calculated using the fluid flux equation (1).

Expressed in terms of the transformed variable, Φ, which is calculated in the solution of the fluid continuity equation, the fluid flux equation is

$$\mathbf{q} = -\underline{\underline{\mathbf{K}}} \left(\frac{\nabla \Phi}{\rho} + \nabla z \right).$$

This equation is discretised by the standard Galerkin finite element method. Treating the material and fluid properties in the same manner as for the fluid continuity equation then leads to the matrix system

$$\begin{aligned} \sum_{J=1}^{nodes} \mathbf{q}^{n+1} \sum_{e} \int_{\Omega^e} N_I N_J d\Omega^e = & - \sum_{J=1}^{nodes} \Phi_J^{n+1} \sum_{e} \frac{\langle \underline{\underline{\mathbf{K}}} \rangle^{n+1}}{\langle \rho \rangle^{n+1}} \int_{\Omega^e} N_I \nabla N_J d\Omega^e \\ & - \sum_{e} \langle \underline{\underline{\mathbf{K}}} \rangle^{n+1} \nabla z \int_{\Omega^e} N_I d\Omega^e \end{aligned}$$

$$(I = 1, 2, \ldots, nodes).$$

The matrix in this system is the finite element mass matrix. The diagonally preconditioned conjugate gradient method, which is very effective for these types of problem [18], is used to solve this system.

The solution of this system gives the nodal approximations to the Darcy velocity vector, which are averaged on each element to generate the elemental approximations, $\langle \mathbf{q} \rangle^{n+1}$.

4.4 Contaminant Mass Balance Equation

Substituting (2) into (3) leads to the following form of the contaminant mass balance equation,

$$\rho\phi\frac{\partial c}{\partial t} + (\rho\mathbf{q}).\nabla c = \nabla.\left\{\phi\underline{\underline{\mathbf{D}}}\nabla(\rho c)\right\}. \tag{10}$$

This is an advection-diffusion equation, which is discretised by the implicit Taylor-Galerkin method outlined in Section 3 by using (10) to replace the temporal derivatives in an approximate Taylor series expansion of the form (8), and then performing a spatial discretisation by the standard Galerkin finite element method.

This leads to the following matrix system which is the fully discretised form of the contaminant mass balance equation

$$\left\{\frac{1}{\Delta t}A + \frac{1}{2}\left(B^{n+1} + C^{n+1}\right)\right\}\mathbf{c}^{n+1} = \left\{\frac{1}{\Delta t}A - \frac{1}{2}\left(B^{n} + C^{n}\right)\right\}\mathbf{c}^{n} - \frac{1}{2}(\mathbf{F}^{n+1} + \mathbf{F}^{n}),$$

where

$$\begin{aligned} A &= \{A^i_{IJ}\}_{I,J=1,\ldots,nodes} & & \\ B^i &= \{B^i_{IJ}\}_{I,J=1,\ldots,nodes} & \mathbf{c}^i &= \{c^i_J\}_{J=1,\ldots,nodes} \\ C^i &= \{C^i_{IJ}\}_{I,J=1,\ldots,nodes} & \mathbf{F}^i &= \{F^i_I\}_{I=1,\ldots,nodes}, \end{aligned}$$

and

$$\begin{aligned} A_{IJ} &= \sum_e A^e_{IJ} = \sum_e \int_{\Omega^e} N_I N_J d\Omega^e \\ B^i_{IJ} &= \sum_e B^{e,i}_{IJ} = \sum_e \int_{\Omega^e} \nabla N_I.\langle\underline{\underline{\mathbf{D}}}\rangle^i \nabla N_J d\Omega^e \\ C^i_{IJ} &= \sum_e C^{e,i}_{IJ} = \sum_e \frac{\langle\mathbf{q}\rangle^i}{\langle\phi\rangle}.\int_{\Omega^e} N_I \nabla N_J d\Omega^e \\ F^i_I &= \sum_e F^{e,i}_I = \sum_e \frac{\langle q^c_n\rangle^i}{\langle\rho\rangle^i\langle\phi\rangle}\int_{\Gamma^e} N_I d\Gamma^e. \end{aligned}$$

The angled brackets have the same meaning as in the discretisation of the fluid continuity equation.

The matrix in this system has three components, the mass matrix A which is symmetric and positive definite, the stiffness matrix B^{n+1} which is symmetric

and positive definite (with the same assumptions on the structure of $\langle \underline{\underline{\mathbf{D}}} \rangle^{n+1}$ as for $\langle \underline{\underline{\mathbf{K}}} \rangle^{n+1}$ in Section 4.2) and the advection matrix C^{n+1} which is non-symmetric and indefinite. Hence the system is non-symmetric and, as with the discrete fluid continuity equation, it is large and sparse.

While a great deal of effort has been expended in the past to avoid producing large sparse non-symmetric matrix systems during numerical algorithms, recent developments in applied linear algebra (e.g. GMRES [14], Bi-CGSTAB [16]) have made it possible to solve such systems efficiently. Bi-CGSTAB is the method used to solve the non-symmetric matrix in this work, with diagonal preconditioning being used to improve the convergence rate.

In all the cases presented in Section 5, the non-symmetric solver converges (where convergence for the system $A\mathbf{u} = \mathbf{f}$ is taken to be when $\|\mathbf{r}\|_2 / \|\mathbf{f}\|_2 \leq 10^{-8}$ and $\mathbf{r} = \mathbf{f} - A\mathbf{u}$) in an acceptable number of iterations (e.g. $\sqrt{n}$, where n is the order of the matrix A). Hence the properties of the discretisation are the only issue considered in the next section.

5 Results

In this section, the algorithm outlined in Section 4 is applied to two standard test cases from the literature; the first involves the 1-D transport of a tracer in a vertical column and the second, which is more specific to the problem of saline intrusion, is the Henry problem.

5.1 Transport of a Tracer in a Vertical Column

This problem involves the 1-D transport of a tracer in a vertical column through which there is a constant fluid flow rate. The physical region, with boundary conditions, for the equivalent 2-D problem is shown in Figure 1 and the data for this problem is :

$$K_{xx} = K_{xz} = K_{zx} = 0 \ , \ K_{zz} = 10^{-4}\text{m/s}$$
$$\phi = 0.2 \ , \ \alpha_L = 5\text{m} \ , \ \alpha_T = 0 \ , \ D_m = 0$$

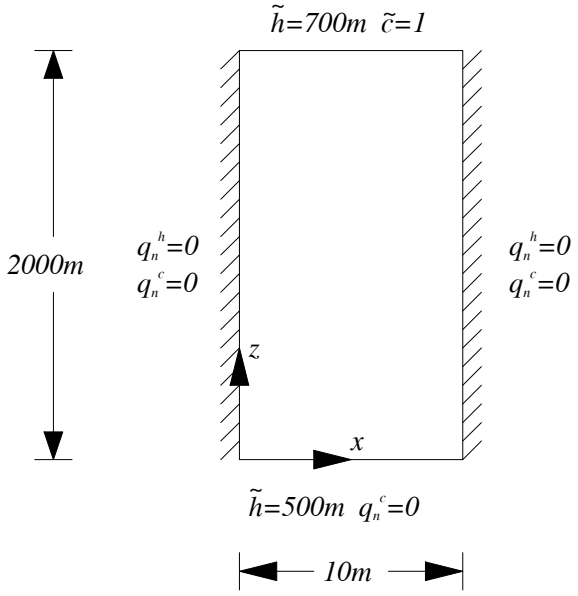

Figure 1: Physical domain and boundary conditions for 1-D problem

In this problem, the transport is passive (i.e. ρ is constant), hence the fluid density cancels from (1), (2) and (3) and does not affect the problem so this quantity is given an arbitrary value. These conditions gives rise to the constant flow field

$$q_x = 0 \qquad q_z = -10^{-5}\text{m/s}$$

The Courant and mesh Peclet numbers for this problem are

$$\nu = \frac{|q_z|}{\phi}\frac{\Delta t}{\Delta z} \qquad Pe = \frac{\Delta z}{\alpha_L}$$

where Δt is the time step and Δz is the vertical mesh size.

Initially, the concentration of the tracer is zero everywhere inside the region. The tracer front moves down the column under the action of gravity and this front disperses as it moves. Until the tracer reaches the bottom of the column, this problem can be analysed as one on a semi-infinite domain in which the boundary conditions are,

$$\begin{aligned} \tilde{c}(x, 2000, t) &= 1 \\ \tilde{c}(x, -\infty, t) &= 0 \\ q_n^c(0, y, t) &= 0 \\ q_n^c(10, y, t) &= 0 \end{aligned}$$

The analytic solution to this problem has been derived in [12] as

$$c(x,z,t) = \frac{1}{2}\left[\exp\left\{\frac{v_z(2000-z)}{D_{zz}}\right\}\mathrm{erfc}\left(\frac{2000-z-v_z t}{2\sqrt{D_{zz}t}}\right) + \mathrm{erfc}\left(\frac{2000-z+v_z t}{2\sqrt{D_{zz}t}}\right)\right]$$

where v_z is the z-component of the fluid velocity vector and erfc is the complementary error function, given by

$$\mathrm{erfc}(s) = \frac{2}{\sqrt{\pi}}\int_s^\infty e^{-u^2}\,du$$

In this work, the complementary error function is computed using the SUNOS C library intrinsic function on a SPARCstation 1+. This problem is solved numerically on a uniform rectangular grid with 401 nodes in the z-direction (and 2 nodes in the x-direction) by the Taylor-Galerkin method from Section 3.2. Figures 2 to 4 show both the approximate (dotted line) and analytic (solid line) solutions, and the error in the solution (defined as the approximate solution minus the analytic solution) for $\Delta t = 5 \times 10^4$ s after 150, 300 and 450 time steps respectively. This corresponds to a Courant number , ν , of 0.5 and a mesh Peclet number, Pe , of 1.0 .

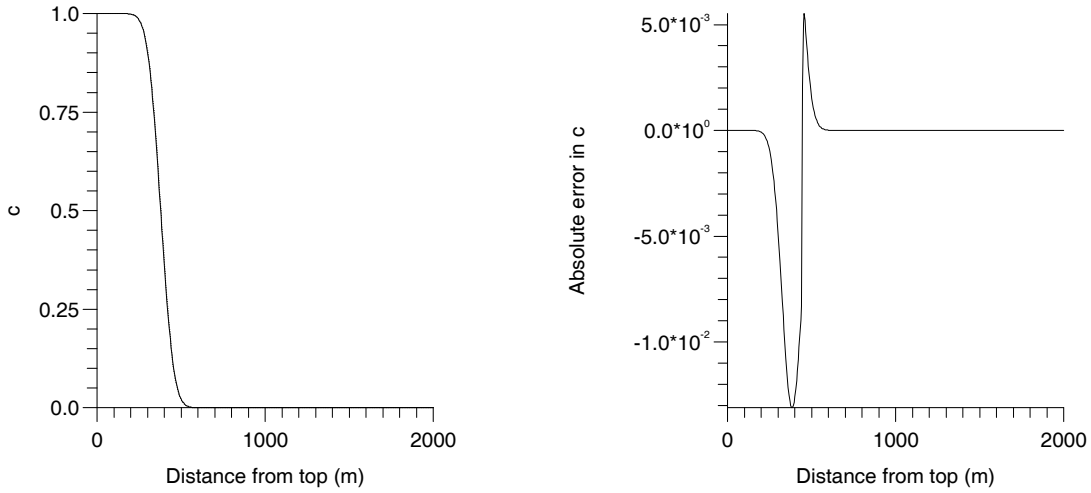

Figure 2: $\nu = 0.5$, $Pe = 1.0$, $t = 7.5 \times 10^6$ s.

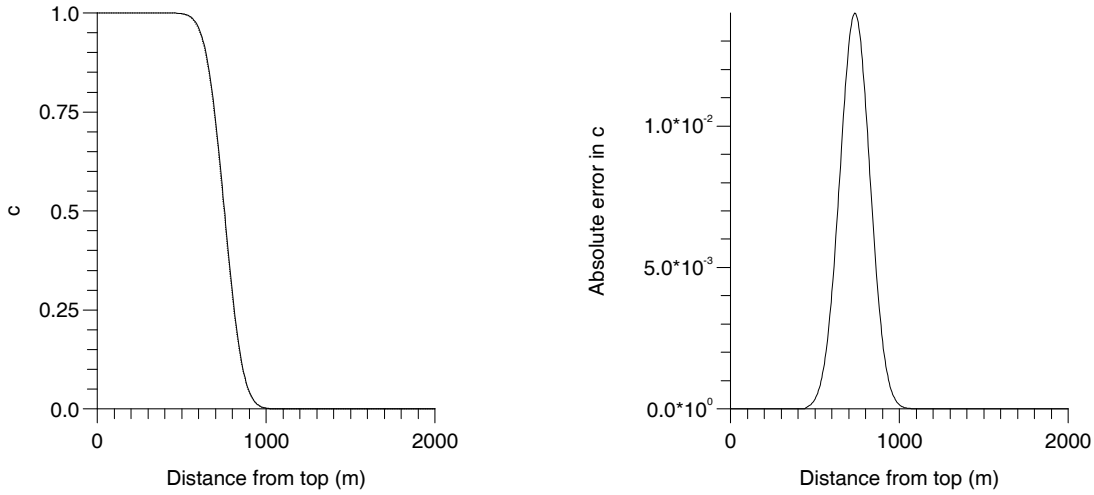

Figure 3: $\nu = 0.5$, $Pe = 1.0$, $t = 1.5 \times 10^7$ s.

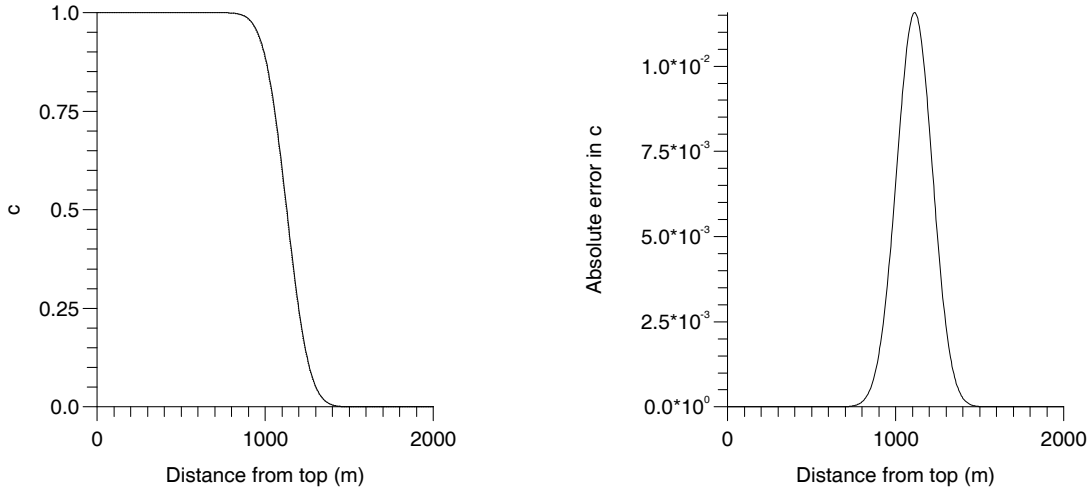

Figure 4: $\nu = 0.5$, $Pe = 1.0$, $t = 2.25 \times 10^7$ s.

Due to the accuracy of the approximate solution, it is hard to distinguish it from the analytic one at each of the times shown. The graphs of the error show the difference more clearly. The solution is monotone and has the correct maximum and minimum values.

Table 1 shows the behaviour of the approximate solution as the Courant number is increased. The maximum and minimum of the approximate solution are shown (to illustrate the possible existence of oscillations). Also shown in the Table is the relative error in the approximate solution

$$\text{Relative Error} = \sqrt{\frac{\sum_i (U_i - u_i)^2}{\sum_i (u_i)^2}},$$

where U is a discrete approximation to u and the subscripts i denote nodal values. For the range of values of Courant number used, the accuracy in the approximation (measured by the relative error) is good.

ν	t	Solution		Relative
	(s)	Minimum	Maximum	Error
0.5	7.5×10^6	0.00000	1.00000	0.007085
	1.5×10^7	0.00000	1.00000	0.006556
	2.25×10^7	0.00000	1.00000	0.004841
1.0	7.5×10^6	0.00000	1.00000	0.016110
	1.5×10^7	0.00000	1.00000	0.001486
	2.25×10^7	0.00000	1.00000	0.000988
5.0	7.5×10^6	0.00000	1.00098	0.030720
	1.5×10^7	0.00000	1.00030	0.010144
	2.25×10^7	0.00000	1.00010	0.007561

Table 1: Effect of varying the Courant number, ν , at $Pe = 1$

It is known that the Crank-Nicolson method is prone to oscillations in front of discontinuities when the Courant number exceeds unity (see e.g. [10]). When the tracer first enters the region, this problem is quite stiff and the tracer front

is almost a discontinuity. To reduce the oscillations this may cause, for the case with $\nu = 5$, the time step is started from $\Delta t = 5 \times 10^4$ s. (corresponding to $\nu = 0.5$) and increased by a factor of 1.2 at each time step to a maximum value of $\Delta t = 5 \times 10^5$ s. (corresponding to $\nu = 5$).

$$\text{i.e. } (\Delta t)_{new} = \min(1.2 \times (\Delta t)_{old}, 5 \times 10^5 \text{ s.})$$

From Table 1, for $\nu = 0.5, 1$ the solution is monotone, but for $\nu = 5$ oscillations in the solution cause un-physical extrema to be created (the maximum value of the dimensionless concentration is greater than one).

Non-physical concentrations can be disastrous in reactive transport models where they affect the chemical terms. Flux-corrected transport methods [2, 19] - i.e. local averaging of the scheme with a positive[1] lower order scheme - may be used in these cases to control the oscillations. However, as this report is not concerned with reactive transport, oscillations are regarded as acceptable as long as they do not cause a serious degradation in the overall quality of the solution.

ν	t	Solution		Relative
	(s)	Minimum	Maximum	Error
0.5	7.5×10^6	0.00000	1.00000	0.025344
	1.5×10^7	0.00000	1.00000	0.005120
	2.25×10^7	0.00000	1.00000	0.003764
1.0	7.5×10^6	0.00000	1.00032	0.078231
	1.5×10^7	0.00000	1.00000	0.036470
	2.25×10^7	0.00000	1.00000	0.026809
5.0	7.5×10^6	0.00000	1.05339	0.229653
	1.5×10^7	0.00000	1.13996	0.111016
	2.25×10^7	0.00006	1.15274	0.103036

Table 2: Effect of varying the Courant number, ν , at $Pe = 5$

In order to investigate the behaviour of the scheme at higher mesh Peclet number (corresponding to problems which are more advection dominated), the

[1]Positivity is the multidimensional generalisation of monotonicity.

grid is changed to one with 81 nodes in the z-direction (this corresponds to a mesh Peclet number of 5). Table 2 shows the behaviour of the approximate solution as the Courant number is increased at $Pe = 5$.

The error in the solution is greater than that in the cases with $Pe = 1$ is expected since both the time step and mesh size are five time greater at $Pe = 5$ than in the equivalent tests at $Pe = 1$.

As before, the scheme is relatively immune to non-physical oscillations when $\nu = 0.5, 1$. However, the scheme is generally more prone to oscillations at this higher mesh Peclet number. This is because the change in concentration at the front is effectively "closer" to a discontinuity since it is resolved on fewer elements. Figure 5 shows the extent of these oscillations in the solution for the case with $\nu = 5.0$ at the intermediate time ($t = 1.5 \times 10^7$ s.).

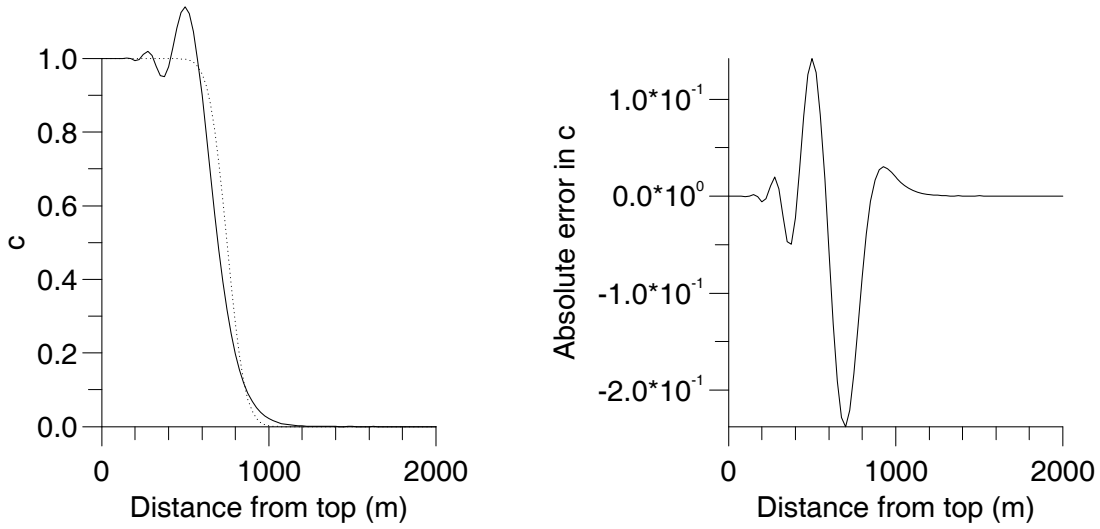

Figure 5: $\nu = 5.0$, $Pe = 5.0$, $t = 1.5 \times 10^7$ s.

5.2 The Henry Problem

The Henry problem [8] is a 2-D, saturated, groundwater flow problem which involves fresh-water in a confined aquifer discharging to a vertical open sea boundary over a diffuse wedge of sea-water that has intruded into the aquifer. An approximate analytic solution to the Henry problem was given in the original paper but no known numerical model matches this solution.

In [17] it is suggested that there may be an inaccuracy in the approximate analytic solution caused by missing higher-order terms which were originally discarded to reduce computation time. Since a large number of numerical models give nearly identical results, this problem has been widely adopted for validation of variable density transport models by comparison with accepted results from the literature.

Figure 6 shows the physical domain and boundary conditions for the Henry problem (where ρ_s is the density of pure sea-water). The confined aquifer is a 2m$\times$1m rectangular region, fresh-water enters on the right side and sea-water enters from the sea boundary on the left side. There can be no flow of water or salt through the horizontal faces.

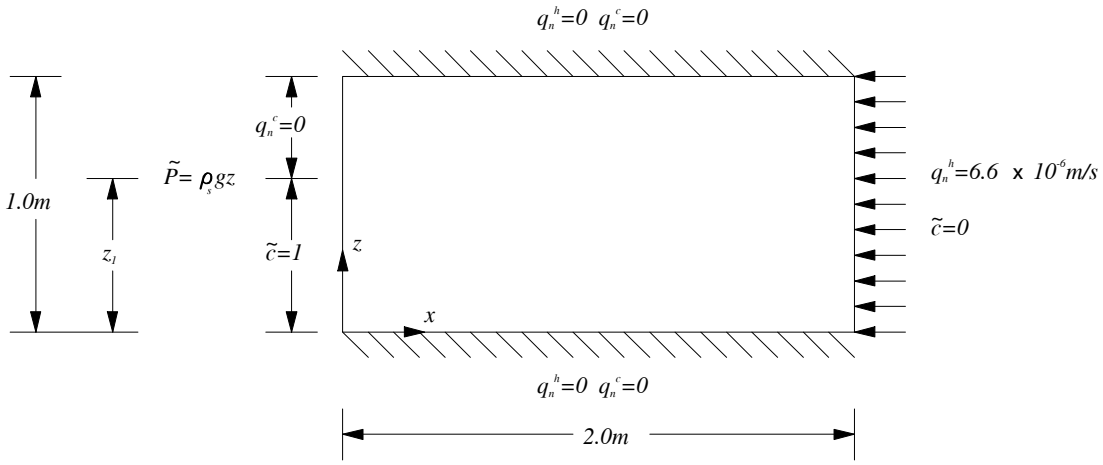

Figure 6: Physical Domain and Boundary Conditions for the Henry Problem

In the original problem, the dimensionless salt concentration is set to unity (i.e. pure sea-water) on the whole of the coastal boundary (the left face). However, this causes a conflict when the freshwater flowing into the region tries to exit at the Dirichlet sea-water face. In accordance with other authors [3, 7, 9, 15], this problem is avoided by changing the coastal boundary condition so that it

consists of two components as shown in Figure 6. On the lower part of the coastal boundary ($0 \leq z \leq z_1$) the dimensionless salt concentration is set to unity, while on the remainder of the coastal boundary ($z_1 < z \leq 1\text{m}$) the prescribed dispersive solute mass flux, q_n^c, is set to zero.

Now z_1 is not known *a priori* but there are two ways of determining this value. In the first (used in e.g. [9]), an initial guess for z_1 is made and a solution is obtained using this initial guess. This solution is analysed and the problem is reformulated but this time with z_1 at the position where the flow on the sea face boundary changes direction from inflow to outflow, and the problem is solved again. By repeating this procedure iteratively, the steady state position of z_1 is obtained. In the second method, the position of z_1 is determined dynamically (i.e. while the time-stepping is being performed) according to

$$q_x \geq 0 \quad \text{for} \quad 0 \leq z \leq z_1$$
$$q_x < 0 \quad \text{for} \quad z_1 < z \leq 1\text{m}$$

where q_x is the horizontal component of the velocity vector, $\mathbf{q}$. Hence, when the flow is directed into the region, there is a Dirichlet boundary condition on the dimensionless salt concentration, but when the flow is directed out of the region, a Neumann boundary condition applies. Forms of this dynamic boundary condition can be found in [7, 15].

The second method for determining z_1 is used in this work because it allows transient features which depend on the position of z_1 to be modelled and only requires that the problem be solved once.

The values of the physical properties for the standard constant dispersion coefficient Henry problem test case are listed below :

$$g = 9.81 \text{ m/s}^2 \ , \ \mu_0 = 0.001 \text{ Pa s} \ , \ \phi = 0.35$$

$$\rho_0 = 1000 \text{ kg/m}^3 \ , \ \frac{\partial \rho}{\partial c} = 24.99 \text{ kg/m}^3$$

$$\underline{\underline{\mathbf{k}}} = 1.019368 \underline{\underline{\mathbf{I}}} \times 10^{-9} \text{ m}^2 \quad \text{where } \underline{\underline{\mathbf{I}}} \text{ is the } 2 \times 2 \text{ identity matrix}$$

$$\alpha_L = 0 \ , \ \alpha_T = 0 \ , \ D_m = 6.6 \times 10^{-6} \text{ m}^2/\text{s}$$

In this test case, a uniform triangular grid is used with 21 nodes in the x-direction and 11 nodes in the z-direction (giving a total of 400 elements). For this problem, the Courant number is

$$\nu = \frac{|\mathbf{q}|}{\phi}\frac{\Delta t}{\Delta x},$$

and mesh Peclet number is

$$Pe = \frac{|\mathbf{q}|}{\phi \|\underline{\underline{\mathbf{D}}}\|_2}\Delta x,$$

assuming $\nabla\rho$ and $\nabla\underline{\underline{\mathbf{D}}}$ are negligible.

Initially, the salt concentration everywhere inside the region is taken to be zero. As with the test case in Section 5.1, when the salt initially enters the region, the problem is quite stiff so a similar simple time stepping scheme is used - an initial time step of 12s. is gradually increased by a factor of 1.2 to a maximum value of 600s. The initial Courant number and mesh Peclet numbers are 0.254 and 11.336 respectively. At t=100 min., the maximum Courant number is which has occurred during the time history is 2.505 and the maximum mesh Peclet number is the initial value.

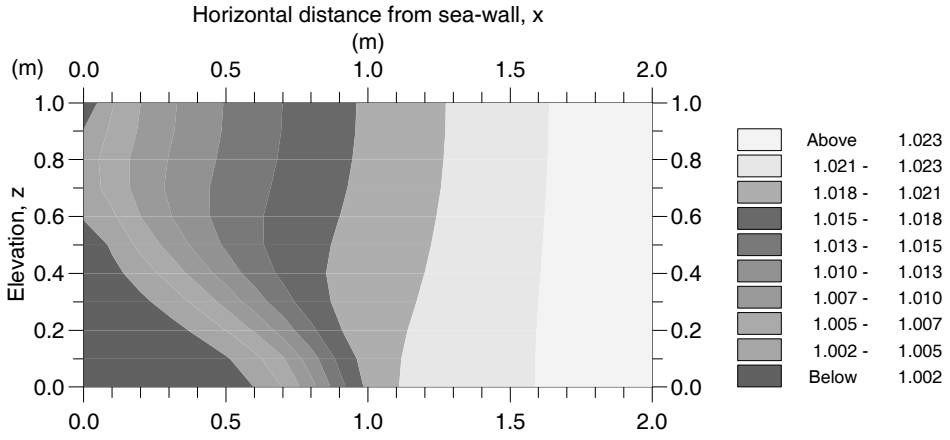

Figure 7: Piezometric pressure head (in m) at t=100 min.

The piezometric pressure head (resulting from the solution of the fluid continuity equation) at t=100 min. is shown in Figure 7 and the Darcy velocity field is shown in Figure 8.

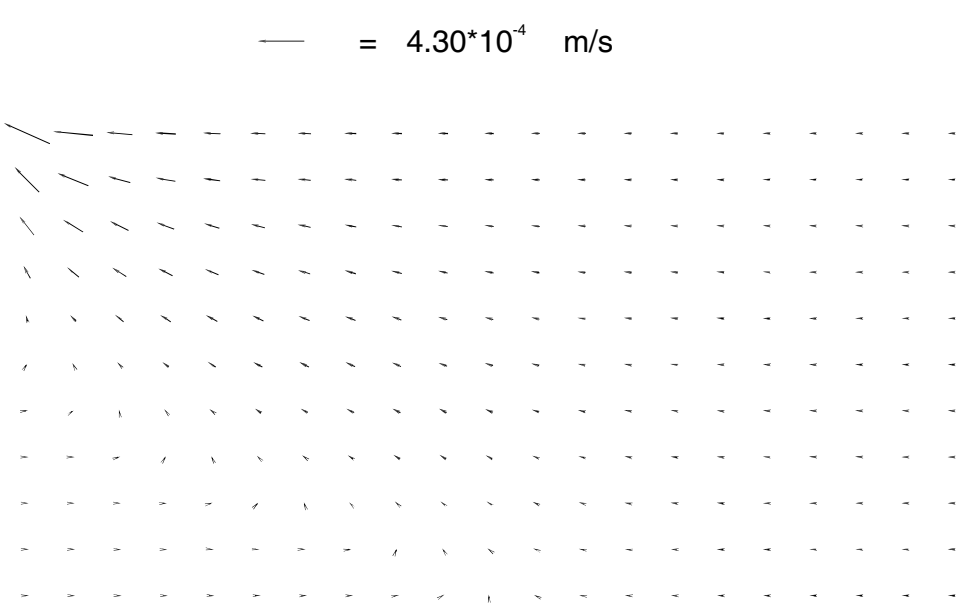

Figure 8: Darcy velocity field (in m/s) at t=100 min.

From Figure 8, the intrusion of the salt-water into the region at the lower part of the left boundary can be seen, as can the entry of freshwater at the right boundary. Most of the freshwater leaves in the upper part of the left boundary but some mixing of the two fluids occurs in the region of varying salt concentration.

Figure 9 shows the positions of the salt isochlors (lines of constant concentration) at t=100 min. The salt forms the expected wedge shape.

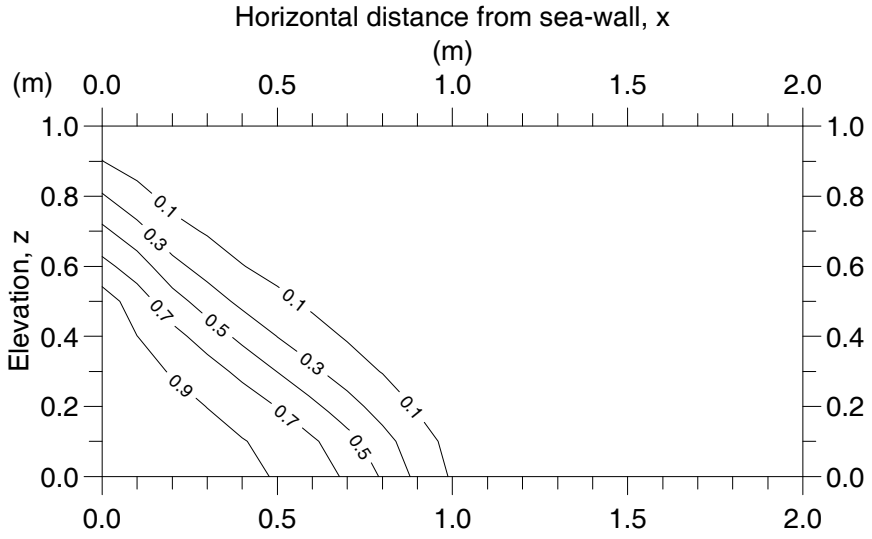

Figure 9: Salt isochlors at t=100 min.

A comparison of the position of the 0.5 isochlor at t=100 min. with the result from [15] is shown in Figure 10 and there is good agreement. A fully coupled approach (i.e. iterating to convergence between the fluid continuity equation and the contaminant continuity equation at each time step) is used in [15], so Figure 10 shows that the partially coupled approach does not seriously affect the accuracy of the approximation for this problem.

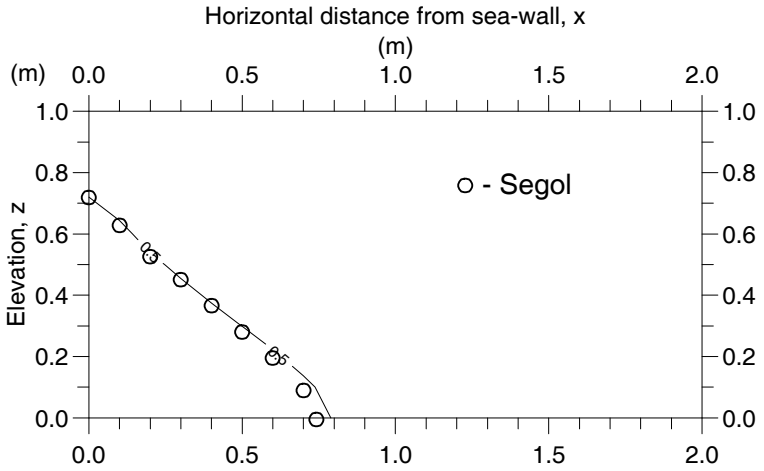

Figure 10: Comparison of position of 0.5 isochlor with [15] at t=100 min.

In order to show the transient accuracy of the algorithm for this problem, the comparison of the position of the 0.5 isochlor at t=30 min. with the result from [15] is shown in Figure 11, and again there is good agreement.

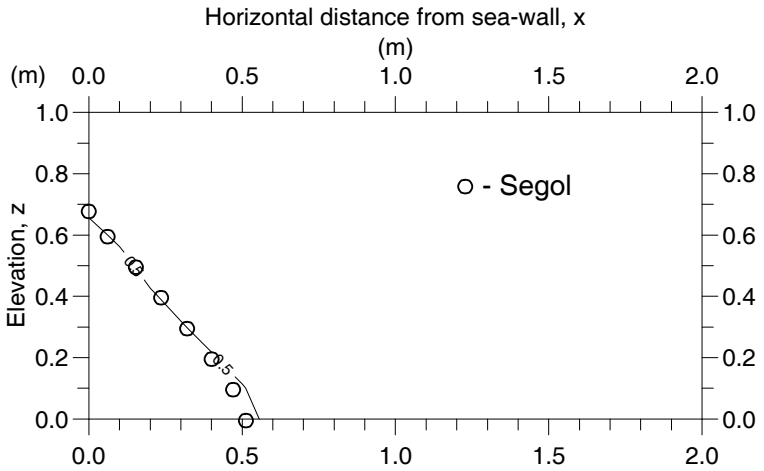

Figure 11: Comparison of position of 0.5 isochlor with [15] at t=30 min.

6 Concluding Remarks

The variable density model for contaminant transport in porous media with a Taylor-Galerkin discretisation for the contaminant continuity equation gives transient results which agree well with analytical solutions and with those from the literature.

The partially coupled approach, in which the weak dependence of the fluid density on the contaminant concentration is exploited by treating the term which causes the coupling between the fluid and contaminant continuity equations (the density) explicitly, is valid for the problems encountered in transient saline intrusion modelling. This approach leads to a substantial decrease in the computational cost.

The fully implicit Taylor-Galerkin method with linear basis functions is equivalent to the Crank-Nicolson finite element method. Although this discretisation method is demonstrated for problems on two-dimensional regular grids in this report, it is fully multi-dimensional and operates on irregular grids in the same way.

For the test cases presented, the diagonally preconditioned Bi-CGSTAB solver converges in an acceptable number of iterations (e.g. $< \sqrt{n}$, where n is the order of the matrix). However, as the Courant number is increased, the advection part of the global matrix (i.e. the component which causes the non-symmetry) becomes more dominant, which may lead to a degradation in the performance of the Bi-CGSTAB solver. The performance of the non-symmetric solver has not been investigated in this report, this aspect of the solution method is the subject of a future study.

7 Acknowledgements

K.J. Neylon is financially supported by a NERC CASE studentship with the collaborating body being the Institute of Hydrology, Wallingford.

He wishes to thank Dr. M.J. Baines, Dr. N.K. Nichols and , in particular, Dr. A. Priestley, of the Mathematics Department, University of Reading, for their advice and assistance during this work.

References

[1] J. Bear and A. Verruijt. *Modeling Groundwater Flow and Pollution.* Reidel, Holland, 1987.

[2] J.P. Boris and D.L. Book. "Flux-corrected transport. I SHASTA, a fluid transport algorithm that works". *JCP*, **11**:38–69, 1973.

[3] L. Brusa, G. Gentile, L. Nigro, D. Mezzani, and R. Rangogni. "A 3-D finite element code for modelling salt intrusion in aquifers". In G. Gambolati, A. Rinaldo, C.A. Brebbia, W.G. Gray, and G.F. Pinder, editors, *Computational Methods in Subsurface Hydrology,* Proc. 8th Int. Conf. on Comp. Meth. in Water Res., Venice, pages 335–340. Springer-Verlag, June 1990.

[4] A.J. Davies. *The Finite Element Method : A First Approach.* Clarendon Press, Oxford, 1980.

[5] J. Donea. "A Taylor-Galerkin method for convective transport problems". *Int. J. Num. Meths. Engng.*, **20**:101–119, 1984.

[6] J. Donea, S. Giuliani, H. Laval, and L. Quartapelle. "Time-accurate solution of advection-diffusion problems by finite elements". *Comp. Meths. App. Mech. Engng.*, **45**:123–145, 1984.

[7] G. Gambolati, G. Galeati, and S.P. Neuman. "A Eulerian-Lagrangian finite element model for coupled groundwater transport". In G. Gambolati, A. Rinaldo, C.A. Brebbia, W.G. Gray, and G.F. Pinder, editors, *Computational Methods in Subsurface Hydrology,* Proc. 8th Int. Conf. on Comp. Meth. in Water Res., Venice, pages 341–347. Springer-Verlag, June 1990.

[8] H.R. Henry. "Effects of dispersion on salt encroachment in coastal aquifers". Water Supply Paper 1613-C:C71-C84, U.S. Geol. Survey, 1964.

[9] P.S. Huyakorn, P.F. Andersen, J.W. Mercer, and White H.O. "Saltwater intrusion in aquifers : Development and testing of a three-dimensional finite element model". *Water Res. Res.*, **23**(2):293–312, 1987.

[10] H.M. Leismann and E.O. Frind. "A symmetric-matrix time integration scheme for the efficient solution of advection-dispersion problems". *Water Res. Res.*, **25**(6):1133–1139, 1989.

[11] J.A. Meijerink and H.A. van der Vorst. "An iterative solution method for linear systems of which the coefficient matrix is a symmetric M-matrix". *Math. Comp.*, **137**(6):148–162, January 1977.

[12] A. Ogata and R.B. Banks. "A solution of the differential equation of longitudinal dispersion in porous media". Professional Paper 411-A, U.S. Geol. Survey, 1961.

[13] A. Priestley. "The Taylor-Galerkin method for the shallow water equations on the sphere". *Monthly Weather Review*, **120**(12):3003–3015, 1992.

[14] Y. Saad and M.H. Schultz. "GMRES : A generalized minimum residual algorithm for solving non-symmetric linear systems". *SIAM J. Sci. Stat. Comput.*, **7**(3):856–869, 1986.

[15] G. Segol, G.F. Pinder, and W.G. Gray. "A Galerkin-finite element technique for calculating the transient position of the saltwater front". *Water Res. Res.*, **6**(3):875–882, 1975.

[16] H.A. van der Vorst. "BI-CGSTAB : A fast and smoothly convergent variant of BI-CG for the solution of nonsymmetric linear systems". *SIAM J. Sci. Stat. Comp.*, **13**(2):631–644, 1992.

[17] C.I Voss and W.R. Souza. "Variable density flow and solute transport simulation of regional aquifers containing a narrow freshwater-saltwater transition zone". *Water Res. Res.*, **23**(10):1851–1866, 1987.

[18] A.J. Wathen. "Realistic eigenvalue bounds for the Galerkin mass matrix". *IMA J. Numer. Anal.*, **7**:449–457, 1987.

[19] S.T. Zalesak. "Fully multidimensional flux-corrected transport algorithms for fluids". *JCP*, **31**:335–362, 1979.